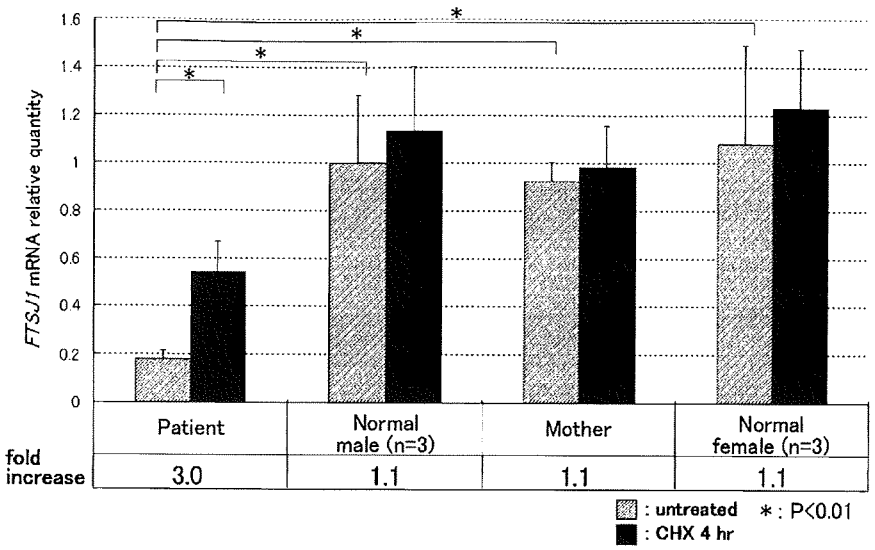

Fig. 6. Quantification of *FTSJ1* mRNA after NMD blockade by CHX treatment. Quantitation of *FTSJ1* mRNA was normalized to *GAPDH* mRNA, with the level in untreated normal males referred to as 1. *FTSJ1* transcripts from the patient's lymphoblast cells showed threefold increase 4 hr after CHX treatment ($P < 0.01$). Smaller increases of *FTSJ1* transcript in the mother and normal controls were not statistically significant ($P > 0.05$). Hatched bars and closed bars indicate samples untreated and 4 hr after CHX treatment, respectively. Representative data from two independent experiments, each run in triplicate, were shown. Statistical analyses were performed using Student's *t*-test. Bars indicate means + SD.

Europeans (2/219 small X-linked families and 2/30 linked families) [Freude et al., 2004; Ramser et al., 2004; Raymond, 2006; Ropers, 2006]. Although it is yet inconclusive, the frequency of *FTSJ1* mutation (2.3%) in one out of 44 Japanese families with at least two MR patients may be compatible with the reported frequency in Europeans. No *FTSJ1* mutation was detected in 29 sporadic MR patients.

Apparently, the c.571 + 1G > A mutation disrupted the consensus for the donor splicing site and accordingly resulted in an aberrantly spliced mRNA. In addition, we observed a significant reduction in the expression of the *FTSJ1* transcripts in the patient's lymphoblast cells in comparison with a normal control, as also found in two previously reported patients [Freude et al., 2004]. These findings are consistent with the prediction that loss-of-function of *FTSJ1* is responsible for the XLMR phenotype associated with *FTSJ1* mutations.

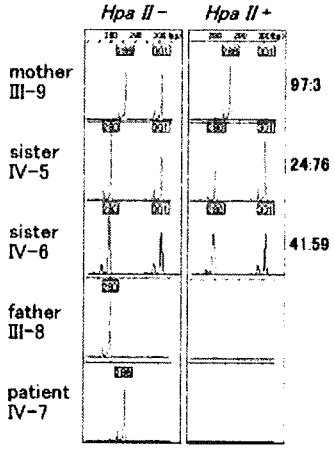

Fig. 7. X chromosome inactivation (XCI) pattern in peripheral leukocytes from the patient's family. XCI pattern was determined by amplification of an androgen receptor (*AR*) polymorphism using genomic DNA undigested and digested with *Hpa II*, indicated by *Hpa II*− and *Hpa II*+, respectively. After enzymatic digestion, only the inactive allele was amplified. The relative peak area of the two alleles after digestion represents the XCI pattern (indicated at right). Digested genomic DNA from the father and patient was not amplified, which indicated complete digestion of unmethylated allele on the active X chromosome. Based on the haplotype at *AR* locus, the recombination event between *AR* and *FTSJ1* loci is unlikely within this pedigree. Each sample was assessed in two independent reactions.

In this study, we further demonstrated why this c.571 + 1G > A mutation resulted in diminished mRNA expression. The major transcript obtained from the patient's lymphoblast cells aberrantly contained entire intron 8 due to the failure of removal from the pre-mRNA. This resulted in a translational read-through into intron 8 and the generation of a PTC in exon 9. This aberrant transcript may become a substrate for NMD, because the predicted PTC is followed by at least 4 introns, which can act as an activating signal for NMD [Holbrook et al., 2004; Maquat, 2004; Wilkinson, 2005]. Accordingly, CHX treatment of patient's cells apparently upregulated *FTSJ1* expression. We assume that the mutant *FTSJ1* mRNA is also degraded in the brain, unless *FTSJ1* is uniquely regulated by differential alternative splicing, or *FTSJ1* escapes NMD specifically in the brain.

The heterozygous mother showed a preferentially skewed XCI pattern in peripheral leukocytes. The skewed XCI pattern has been commonly observed in carrier female leukocytes from families with XLMR disorders [Plenge et al., 2002] and may occur as a result of the mutation of the genes that might adversely affect cell survival or proliferation [Belmont, 1996; Willard, 1996]. Although the mechanism triggering the skewing pressure preferentially in the mother remain unknown, the *FTSJ1* mutation in the carrier females may also have resulted in a skewed pattern of XCI like other XLMR disorders.

FTSJ1 is a human homolog of the *Escherichia coli 2'-O*-rRNA methyltransferase FtsJ/RrmJ gene [Bügl et al., 2000; Pintard et al., 2000]. Based on studies in lower organisms, FtsJ binds S-adenosylmethionine (SAM) [Bügl et al., 2000], methylates rRNA [Bügl et al., 2000; Pintard et al., 2002a], modifies tRNA [Pintard et al., 2002b] and probably plays an essential role in translation. Although the function of *FTSJ1* in human is yet unknown, FtsJ is well conserved from bacteria to human. SAM is the major methyl donor for cellular methyltransferase reactions, and low SAM concentration in cerebrospinal fluid or

plasma was observed in several neuropsychiatric and neurological disorders including autism [James et al., 2004; Ramser et al., 2004]. Therefore, predicted impairment of binding to SAM due to the loss-of-function of *FTSJ1* may have potential consequences in MR phenotype. Despite the fact that *FTSJ1* is ubiquitously expressed in a broad range of human tissue [Freude et al., 2004; Ramser et al., 2004], loss-of-function mutation of *FTSJ1*, including our case, caused relatively mild MR without apparent morphologic abnormalities in the brain or other non-neurologic symptoms, suggesting that mutations in the *FTSJ1* gene only affect cognitive function in human. Three homologues of FtsJ, *FTSJ1*, *FTSJ2* [Ching et al., 2002], and *FTSJ3*, are present in human, and they contain a highly conserved Ftsj domain [Ramser et al., 2004]. Both *FTSJ2* [Ching et al., 2002] and *FTSJ3* (NCBI GEO DataSet GDS 2190, 1663) are also expressed ubiquitously in most tissues including brain. Although the cellular expression pattern of each FtsJ homolog is yet undetermined, it is possible that co-present normal *FTSJ2* and *FTSJ3* compensate for loss-of-function of *FTSJ1*.

In conclusion, we identified a novel splice site mutation in *FTSJ1* gene causing NS-XLMR in a Japanese family. The frequency of *FTSJ1* mutation in Japanese MR families may be approximately the same as in Europeans. Since we demonstrated that this mutation resulted in a significant decrease of *FTSJ1* transcript, loss-of-function is the likely mechanism for the clinical phenotype of this family. Further investigation of the function of the *FTSJ1* gene in the human brain may serve to elucidate the pathoetiological basis of cognitive dysfunction present in patients with XLMR.

ACKNOWLEDGMENTS

This work is part of an ongoing study by the Japanese Mental Retardation Research Consortium. We thank the patients and families for their generous participation in this study, N. Murakami for cell culture and EBV-transformation, and M. Kato, C. Hemmi, and Y. Sawano for technical assistance. This work was supported in part by the research grant (15B-4, 18A-5) for Nervous and Mental Disorders from the Ministry of Health, Labour and Welfare, Japan (Y-i.G.) and Grants-in-Aid for Scientific Research (1739012) from the Japan Society for the Promotion of Science, Japan (K.I.).

REFERENCES

Allen RC, Zoghbi HY, Moseley AB, Rosenblatt HM, Belmont JW. 1992. Methylation of *HpaII* and *HhaI* sites near the polymorphic CAG repeat in the human androgen-receptor gene correlates with X chromosome inactivation. Am J Hum Genet 51:1229–1239.

Belmont JW. 1996. Genetic control of X inactivation and processes leading to X-inactivation skewing. Am J Hum Genet 58:1101–1108.

Bügl H, Fauman EB, Staker BL, Zheng F, Kushner SR, Saper MA, Bardwell JCA, Jakob U. 2000. RNA methylation under heat shock control. Mol Cell 6:349–360.

Carter MS, Doskow J, Morris P, Li S, Nhim RP, Sandstedt S, Wilkinson MF. 1995. A regulatory mechanism that detects premature nonsense codons in T-cell receptor transcripts in vivo is reversed by protein synthesis inhibitors in vitro. J Biol Chem 270:28995–29003.

Chelly J, Mandel JL. 2001. Monogenic causes of X-linked mental retardation. Nat Rev Genet 2:669–680.

Ching YP, Zhou HJ, Yuan JG, Qiang BQ, Kung HF, Jin DY. 2002. Identification and characterization of FTSJ2, a novel human nucleolar protein homologous to bacterial ribosomal RNA methyltransferase. Genomics 79:2–6.

Darlington GJ. 1998. Isolation and transformation of lymphocytes. New York: Cold Spring Harbor Laboratory Press. pp 7.1–7.5.

Fishburn J, Turner G, Daniel A, Brookwell R. 1983. The diagnosis and frequency of X-linked conditions in a cohort of moderately retarded males with affected brothers. Am J Med Genet 14:713–724.

Freude K, Hoffmann K, Jensen LR, Delatycki MB, des Portes V, Moser B, Hamel B, van Bokhoven H, Moraine C, Fryns JP, Chelly J, Gécz J, Lenzner S, Kalscheuer VM, Ropers HH. 2004. Mutations in the *FTSJ1* gene coding for a novel S-adenosylmethionine-binding protein cause nonsyndromic X-linked mental retardation. Am J Hum Genet 75:305–309.

Holbrook JA, Neu-Yilik G, Hentze MW, Kulozik AE. 2004. Nonsense-mediated decay approaches the clinic. Nat Genet 36:801–808.

Inoue K, Khajavi M, Ohyama T, Hirabayashi S, Wilson J, Reggin JD, Mancias P, Butler IJ, Wilkinson MF, Wegner M, Lupski JR. 2004. Molecular mechanism for distinct neurological phenotypes conveyed by allelic truncating mutations. Nat Genet 36:361–369.

James SJ, Cutler P, Melnyk S, Jernigan S, Janak L, Gaylor DW, Neubrander JA. 2004. Metabolic biomarkers of increased oxidative stress and impaired methylation capacity in children with autism. Am J Clin Nutr 80:1611–1617.

Kaga M, Horiguchi T, Inagaki M. 2002. Early detection and therapeutic rearing for children with mental retardation: I. Assessment of diagnosing examination and collaborative facilities assigned for children with mental retardation. No To Hattatsu 34:235–242.

Leonard H, Wen X. 2002. The epidemiology of mental retardation: Challenges and opportunities in the new millennium. Ment Retard Dev Disabil Res Rev 8:117–134.

Maquat LE. 2004. Nonsense-mediated mRNA decay: Splicing, translation and mRNP dynamics. Nat Rev Mol Cell Biol 5:89–99.

Murphy RM, Watt KKO, Cameron-Smith D, Gibbons CJ, Snow RJ. 2003. Effects of creatine supplementation on housekeeping genes in human skeletal muscle using real-time RT-PCR. Physiol Genomics 12:163–174.

Nanba E, Kohno Y, Matsuda A, Yano M, Sato C, Hashimoto K, Koeda T, Yoshino K, Kimura M, Maeoka Y, Yamamoto T, Maegaki Y, Eda I, Takeshita K. 1995. Non-radioactive DNA diagnosis for the fragile X syndrome in mentally retarded Japanese males. Brain Dev 17:317–321.

Noensie EN, Dietz HC. 2001. A strategy for disease gene identification through nonsense-mediated mRNA decay inhibition. Nat Biotechnol 19:434–439.

Pintard L, Kressler D, Lapeyre B. 2000. Spb1p is a yeast nucleolar protein associated with Nop1p and Nop58p that is able to bind S-adenosyl-L-methionine in vitro. Mol Cell Biol 20:1370–1381.

Pintard L, Bujnicki JM, Lapeyre B, Bonnerot C. 2002a. *MRM2* encodes a novel yeast mitochondrial 21S rRNA methyltransferase. EMBO J 21: 1139–1147.

Pintard L, Lecointe F, Bujnicki JM, Bonnerot C, Grosjean H, Lapeyre B. 2002b. Trm7p catalyses the formation of two 2'-*O*-methylriboses in yeast tRNA anticodon loop. EMBO J 21:1811–1820.

Plenge RM, Stevenson RA, Lubs HA, Schwartz CE, Willard HF. 2002. Skewed X-chromosome inactivation is a common feature of X-linked mental retardation disorders. Am J Hum Genet 71:168–173.

Ramser J, Winnepenninckx B, Lenski C, Errijgers V, Platzer M, Schwartz CE, Meindl A, Kooy RF. 2004. A splice site mutation in the methyltransferase gene *FTSJ1* in Xp11.23 is associated with non-syndromic mental retardation in a large Belgian family (MRX9). J Med Genet 41:679–683.

Raymond FL. 2006. X linked mental retardation: A clinical guide. J Med Genet 43:193–200.

Ropers HH. 2006. X-linked mental retardation: Many genes for a complex disorder. Curr Opin Genet Dev 16:260–269.

Ropers HH, Hamel BCJ. 2005. X-linked mental retardation. Nat Rev Genet 6:46–57.

Wilkinson MF. 2005. A new function for nonsense-mediated mRNA-decay factors. Trends Genet 21:143–148.

Willard HF. 1996. X chromosome inactivation and X-linked mental retardation. Am J Med Genet 64:21–26.

J Hum Genet
DOI 10.1007/s10038-008-0289-8

ORIGINAL ARTICLE

Genotype and phenotype analyses in 136 patients with single large-scale mitochondrial DNA deletions

Shintaro Yamashita · Ichizo Nishino · Ikuya Nonaka · Yu-ichi Goto

Received: 1 February 2008 / Accepted: 17 March 2008

Abstract We examined 136 patients with mitochondrial DNA (mtDNA) deletion. Clinical diagnoses included chronic progressive external ophthalmoplegia (94 patients); Kearns–Sayre syndrome (KSS; 33 patients); Pearson's marrow-pancreas syndrome (six patients); and Leigh syndrome, Reye-like syndrome, and mitochondrial myopathy, encephalopathy, lactic acidosis, and stroke-like episodes (one patient). The length and location of deletion were highly variable. Only one patient had deletion within the so-called shorter arc between the two origins of mtDNA replication. The length of deletion and the number of deleted transfer ribonucleic acid (tRNAs) showed a significant relationship with age at onset. Furthermore, KSS patients had longer and larger numbers of deleted tRNAs, which could be risk factors for the systemic involvement of single mtDNA deletion diseases. We found 81 patterns of deletion. Direct repeats of 4 bp or longer flanking the breakpoints were found in 96 patients (70.5%) and those of 10 bp or longer in 49 patients (36.0%). We found two other common deletions besides the most common deletion (34 patients: 25.0%): the 2,310-bp deletion from nt 12113 to nt 14421 (11 patients: 8.0%) and the 7,664-bp deletion from nt 6330 to nt 13993 (ten patients: 7.3%). These deletions had incomplete direct repeats longer than 13 bp with one base mismatch.

Keywords Mitochondrial DNA · Deletion · CPEO · KSS · Direct repeat

S. Yamashita · Y. Goto (✉)
Department of Mental Retardation and Birth Defect Research,
National Institute of Neuroscience,
National Center of Neurology and Psychiatry (NCNP),
4-1-1 Ogawahigashi, Kodaira, Tokyo 187-8502, Japan
e-mail: goto@ncnp.go.jp

I. Nishino · I. Nonaka
Department of Neuromuscular Research,
National Institute of Neuroscience,
National Center of Neurology and Psychiatry (NCNP),
Kodaira, Tokyo, Japan

S. Yamashita
Department of Pediatrics and Adolescent Medicine,
Juntendo University School of Medicine,
Bunkyo-ku, Tokyo, Japan

Introduction

Mitochondria are organelles found in every cell except in mature erythrocytes, and they function as an energy-converting factory. Mitochondrial dysfunction causes organ damage producing various clinical symptoms due to energy crisis in a cell. Nuclear gene and mitochondrial DNA (mtDNA) mutations are thought to be related to mitochondrial disease. MtDNA mutations are classified to depletion, deletion/duplication, and point mutations.

Deletions of the mtDNA were the first mutations reported in association with human disease (Holt et al. 1988). Some patients have duplications of mtDNA as well as deletions (Poulton et al. 1989). Subsequently, multiple mtDNA deletions have been described in familial cases (Zeviani et al. 1989; Servidei et al. 1991), and nuclear gene defects predisposing to multiple deletions have been documented (Nishino et al. 1999; Kaukonen et al. 2000; Van Goethem et al. 2001; Spelbrink et al. 2001).

Single large-scale deletions of mtDNA are typically associated with chronic progressive external ophthalmoplegia (CPEO), Kearns–Sayre syndrome (KSS), and Pearson's marrow-pancreas syndrome (PS) (Holt et al. 1988; Zeviani et al. 1988; Rötig et al. 1989; Campos et al.

2000; Akman et al. 2004). Deletions exist in a heteroplasmic fashion, and the proportion of heteroplasmy is variable among cells and organs. Although a common 4,977-bp deletion is present (Schon et al. 1989), there appears to be many other deletions differing in length and position. Frequently, sequences at the breakpoints revealed the presence of direct repeats, suggesting the mechanism of deletion as slipped mispairing or homologous recombination (Shoffner et al. 1989; Mita et al. 1990).

In this study, we examined 136 Japanese patients with single large-scale mtDNA deletions for the clinical phenotypes and genomic characteristics of deletion, including the precise junction sequences to delineate genotype–phenotype correlation. Furthermore, we provided fundamental clinical information of the single large-scale mtDNA deletion disorder.

Patients and methods

Patients

Between 1987 and 2005, we examined 136 patients who had single large-scale deletions in the mtDNA obtained from the skeletal muscle or peripheral blood. Among 136 DNA samples, eight (six PS and two CPEO) were blood and the remaining 128 samples were all skeletal muscle. The result of muscle DNA was exclusively utilized to assess the relationship between the heteroplasmy and the age at onset. All patients gave informed consent before muscle biopsy or mtDNA analysis was performed. Clinical data, including clinical manifestations and laboratory findings, were obtained from the attending physicians at the time of muscle biopsy or mtDNA analysis. Some of the patients were previously described (Goto et al. 1990a, b; Nakai et al. 1994; Mori et al. 1991).

Detection of mtDNA deletions by Southern blot analysis, long polymerase chain reaction, and sequence determination of breakpoints

DNA samples from muscle biopsies were prepared by the method described previously (Goto et al. 1990a) and those from peripheral blood by the method of Miller et al. (1988). Southern blot analysis was performed according to the method described previously (Goto et al. 1990a). The proportion of the deleted mtDNA was measured by densitometrical analysis. Long polymerase chain reaction (PCR) amplification and junction sequence determination at breakpoints were performed as described previously (Goto et al. 1996).

Statistical analysis

To compare the quantitative parameters between two groups, we used the Mann–Whitney U test. A P value <0.05 was considered significant. We considered results of correlation coefficient as follows: between the range of ± 0 and ± 0.2 as no correlation, ± 0.2 and ± 0.4 as weak correlation, ± 0.4 and ± 0.7 as moderate correlation, and ± 0.7 and ± 1.0 as significant correlation.

Results

Clinical diagnosis

Sixty male and 76 female patients were included in the study. No family history was identified except in two patients who derived from the same family (Ozawa et al. 1988). Clinical diagnoses included CPEO in 94 patients (69%), KSS in 33 (24%), PS in six(4%), and others in three (2%). We adopted the criteria of KSS proposed by Rowland (1983). All KSS patients had ophthalmoplegia, pigmentary retinopathy, onset before age 20, and one of the following: complete heart conduction block, high cerebrospinal fluid protein content, and cerebellar symptoms. Diagnosis of PS was made based on the presence or absence of anemia and/or vacuoles in erythroblasts or other hematologic cell lineages and pancreatic dysfunction. Major manifestations and selected laboratory findings of each clinical diagnosis are summarized in Table 1.

Clinical manifestations and laboratory findings

The incidence of major clinical manifestations and laboratory findings are summarized in Table 1. Ptosis/PEO was collectively found in 94% of patients, muscle weakness in 87%, retinopathy in 34%, heart conduction block in 24%, deafness in 30%, and short stature in 26%. Major laboratory findings, including high CK, high lactate levels in serum and cerebrospinal fluid (CSF), and increased CSF protein content, were detected in more than one third to almost one half of patients. Compared with CPEO, KSS had a high frequency of retinopathy, heart conduction block, and increased CSF protein content because of Rowland's criteria. However, it was notable that deafness (64%) and short stature (70%) were frequently observed in KSS, and insulin-dependent diabetes mellitus (IDDM) (15%) and deToni–Fanconi–Debré syndrome (12%) were sometimes prominent complications in KSS. Because we encountered only six PS patients, it was difficult to compare the incidence of major symptoms and laboratory findings with other phenotypes.

Table 1 Clinical manifestations and major laboratory data

Clinical diagnosis	Number	Clinical manifestation							Laboratory data			
		Ptosis/PEO	Muscle weakness	Retinopathy	Heart conduction block	Deafness	Short stature	Anemia	IDDM	High CK	High lactate		Increased CSF protein
											Serum	CSF	
CPEO (%)	94	94/94 (100)	76/94 (81)	5/71 (70)	8/78 (10)	15/83 (18)	13/94 (14)	0/94 (0)	1/94 (1)	27/83 (33)	23/83 (28)	16/63 (25)	22/66 (33)
KSS (%)	33	33/33 (100)	26/33 (79)	33/33 (100)	20/33 (61)	21/33 (64)	23/33 (70)	0/33 (0)	5/33 (15)	9/26 (35)	22/32 (69)	19/25 (76)	24/25 (96)
PS	6	1/6	1/3	0/2	0/3	0/3	0/6	6/6	1/6	0/4	4/5	2/3	1/2
Others	3	0/3	3/3	0/3	0/3	0/1	0/3	1/3	0/3	0/3	2/3	3/3	1/3
Total (%)	136	128/136 (94)	116/133 (87)	37/109 (34)	28/117 (24)	36/120 (30)	36/136 (26)	7/136 (5)	7/136 (5)	36/116 (31)	50/123 (41)	40/94 (43)	48/96 (50)

Number of patients who had clinical manifestation or laboratory data/number of patients whose data we obtained

PEO progressive external ophthalmoplegia, *KSS* Kearns–Sayre syndrome, *PS* Pearson syndrome, *IDDM* insulin-dependent diabetes mellitus, *CK* creatine kinase, *CSF* cerebrospinal fluid

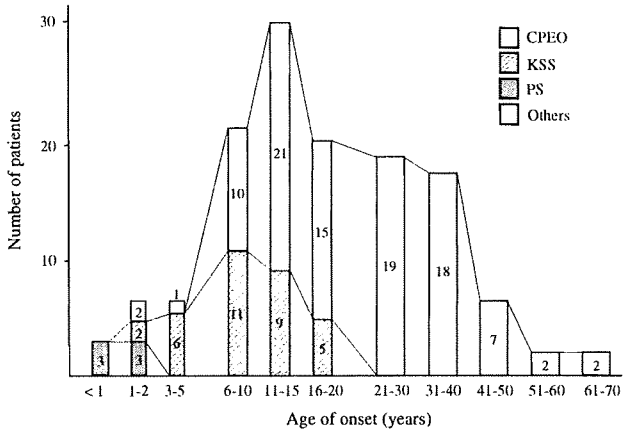

Fig. 1 Distribution of age at onset in various clinical forms. *CPEO* chronic progressive external ophthalmoplegia, *KSS* Kearns–Sayre syndrome, *PS* Pearson's marrow-pancreas syndrome

Age at onset and initial symptoms

Age at onset ranged from birth to 65 (19.8 ± 13.9) years. Figure 1 shows the distribution of age at onset in CPEO, KSS, PS, and other diseases. In 88 patients (65%), disease onset was before the age of 20 years.

Of the 94 CPEO patients, all were older than 6 years. As for their initial symptoms, 88 patients (94%) showed PEO, five patients showed muscle weakness, and only one patient showed deafness. Although the age at onset in the 33 KSS patients was from 1 to 19 years based on Rowland's criteria, 22 (67%) had ptosis or PEO or muscle weakness. The initial findings of the patients whose age at onset was younger than 5 years were short stature and IDDM but not ptosis or PEO. One patient whose initial finding was short stature exhibited rare renal tubular dysfunction mimicking Bartter syndrome and subsequently typical ptosis and PEO (Goto et al. 1990b). All six PS patients were younger than 2 years and did not have PEO at the time of diagnosis.

Three patients with atypical phenotype

Three patients showed the following atypical and severe clinical phenotypes: mitochondrial myopathy, encephalopathy, lactic acidosis and stroke-like episodes (MELAS), Leigh syndrome, and Reye-like syndrome.

The first patient was a 4-year-old boy. He experienced status epilepticus and syndrome of inappropriate secretion of antidiuretic hormone (SIADH) accompanied by abdominal pain and vomiting when he was 2 years old. Thereafter, he periodically had abdominal pain and vomiting once or twice a year. At 4 years and 10 months of age, he showed a stroke-like episode with disturbance of consciousness, convulsions, and severe metabolic acidosis.

Cranial computed tomography showed a low-density area in the occipital lobes. The lactate level in serum was slightly increased (16.5 mg/dl: normal <15) and that in CSF was significantly increased (41.7 mg/dl). Muscle biopsy showed some ragged-red fibers but not strongly succinate-dehydrogenase -reactive blood vessels (SSVs). On cytochrome *c* oxidase (COX) staining, scattered fibers with no enzyme activity were observed, suggesting focal COX deficiency. Based on these findings, we considered that MELAS was the most likely diagnosis, as neither 3243 nor 3271 mutation, which is frequently detected in MELAS patients, was found in this case.

The second patient was a 2-year-old boy. During the perinatal period, he developed pancytopenia that required treatment. His psychomotor development was within the normal range, but he showed a sudden seizure with unconsciousness and motor disturbance followed by viral gastroenteritis. Cranial magnetic resonance imaging (MRI) showed T1 low intensity and T2 high intensity in the thalamus and basal ganglia. Serum and CSF lactate levels were significantly increased (32 and 43 mg/dl, respectively). Muscle biopsy showed no typical ragged-red fibers. On COX staining, the enzyme activity was mildly and diffusely decreased. We considered that Leigh syndrome was the most likely diagnosis for this patient.

The third patient was a 1.5-year-old boy. After an episode of vomiting and diarrhea probably due to gastroenteritis, he developed abrupt systemic edema following continuous tonic and clonic seizures. Laboratory findings showed hypoproteinemia, hypoglycemia, severe ketoacidosis with high lactate level, and liver dysfunction. MRI and organic acid and amino acid analyses showed no apparent abnormality. Liver biopsy showed small vacuoles in hepatocytes, suggesting steatosis. Muscle biopsy showed a few ragged-red fibers, and no SSVs were detected. On COX staining, fibers with no enzyme activity were occasionally observed. The patient was diagnosed as having Reye-like syndrome because he lacked specific symptoms or laboratory findings suggestive of CPEO, KSS, and PS.

Because all three patients were younger than 4 years old at the time of examination, we could not exclude the possibility that they might show other symptoms or laboratory findings indicative of CPEO, KSS, and PS in the future.

Length and location of deletion

The length and location of deletion were highly variable. The length of deletion in 135 patients ranged from 1.1 to 9.6 kilobases (kb) (5.1 ± 1.6 kb on average). The breakpoints of the left borders were located from nt 5834 to nt 13911 and those of the right borders from nt 9519 to nt 16123, which distributed throughout the entire longer arc

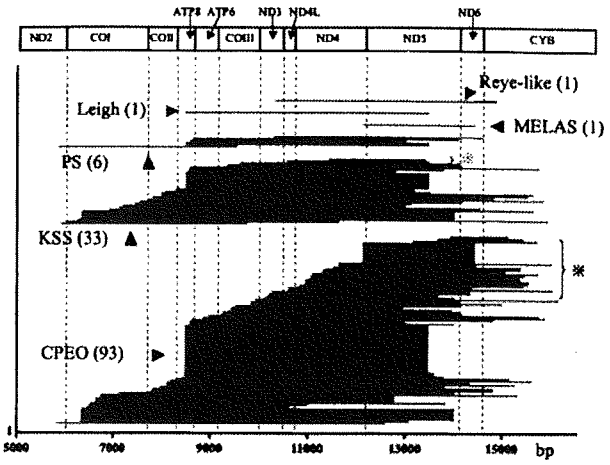

Fig. 2 Localization of 135 deletions. *ND* complex I subunit, *CO* complex IV subunit, *ATP* adenosine triphosphate synthase subunit, *MELAS* mitochondrial myopathy, encephalopathy, lactic acidosis, and stroke-like episodes, ※ = patients with deletion encompassing only ND or ND plus cytochrome b (CYB) subunits

of mtDNA (Fig. 2). Only one patient had deletion within the so-called shorter arc between the two origins of mtDNA replication (nucleotide numbers 191–5730). The deletion was from nt 548 to nt 4442, including one protein-coding subunit (ND1), five complete and one incomplete transfer ribonucleic acid (tRNA) regions, and a part of the control region. The similar deletion had already been reported (Hammans et al. 1992).

We noted that the short deletions or deletions encompassing only complex I (ND) subunits might be more frequent in CPEO than in KSS (Fig. 2). To confirm this finding, we examined all patients except atypical cases (PS, MELAS, Leigh syndrome, Reye-like syndrome, and CPEO patients who have deletion at the shorter arc) regarding the relationship between age at onset and the following:

1. Length of deletion
   We first examined the relationship between the length of deletion and the age at onset. The result suggests a moderate correlation (correlation coefficient $r = -0.51$; Fig. 3). Furthermore, we compared the length of deletion between CPEO and KSS patients. KSS patients seemed to have significantly longer deletion than CPEO patients ($P = 0.005 < 0.01$).
2. Number of deleted tRNAs
   Although the number of deleted tRNAs might be associated with the length of deletion, we examined the relationship between the number of deleted tRNAs and the age at onset. The result suggests a moderate correlation (correlation coefficient $r = -0.48$; Fig. 4). Furthermore, we compared the number of deleted tRNAs and the age at onset between CPEO and KSS patients. KSS patients seemed to have significantly

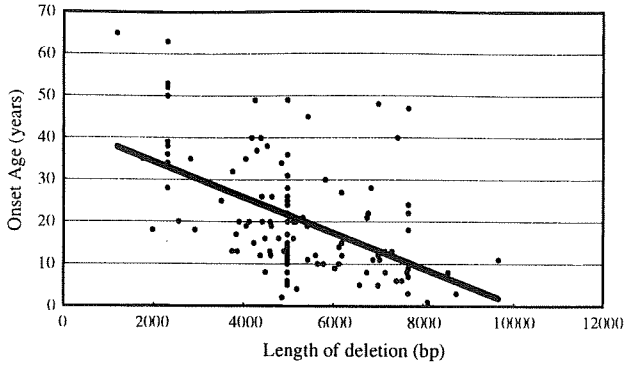

Fig. 3 Scattergram and linear regression between the length of mitochondrial DNA (mtDNA) deletion and age at onset

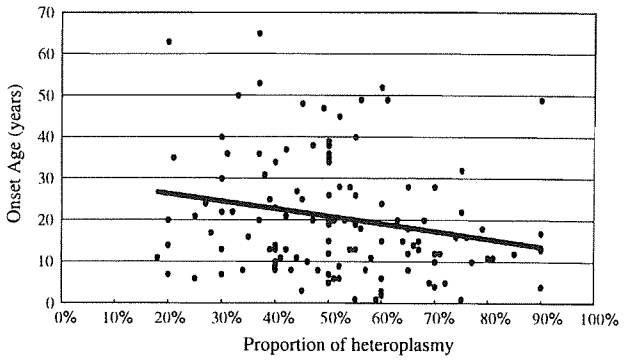

Fig. 5 Scattergram and linear regression between the proportion of deleted mitochondrial DNA (mtDNA) and age at onset

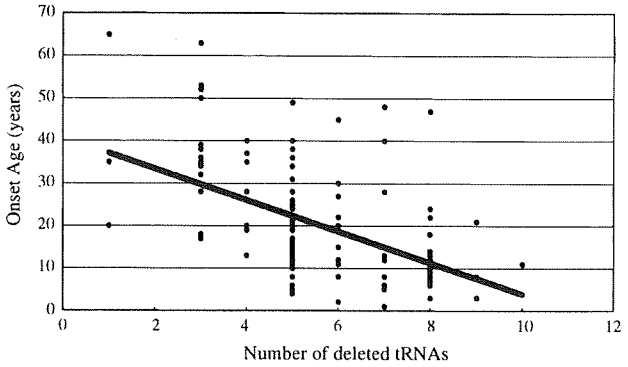

Fig. 4 Scattergram and linear regression between the number of deleted tRNAs and age at onset

more deleted tRNAs than CPEO patients ($P = 0.008 < 0.01$).

3. Location of deletion
   The deletion sometimes included only ND subunits or ND plus cytochrome b (CYB) subunits, sparing COX and adenosine triphosphate (ATP) synthase subunits (Fig. 2). To determine the relationship between the location of deletion and the age at onset, we divided the patients to group 1 (with deletion encompassing only ND or ND plus CYB subunits) and group 2 (with deletion encompassing at least one COX or ATP subunit). Group 1 consisted of 27% of the patients, whereas group 2 consisted of 73% of patients. The age at onset between groups 1 and 2 showed a statistical significance ($P < 0.0001$).

Proportion of deleted mtDNA

To assess whether heteroplasmy might play a role in phenotypic manifestation, we determined the proportion of deleted mtDNA in skeletal muscle samples from 128 patients on Southern blot analysis. It ranged from 18% to 90% (52.2 ± 16.8%), but only a slight correlation between heteroplasmy and age at onset (correlation coefficient $r = -0.21$; Fig. 5) was evident. To exclude the effects of the differences in length and position as much as possible, we compared patients having the same deletion, or the so-called common 4,977-bp deletion. There were no correlations among age at onset, clinical diagnosis, clinical manifestation, and heteroplasmy (Table 2).

Sequences of deletion breakpoints

In this study, we found 81 patterns of mtDNA deletion. Direct repeats of 4 bp or longer flanking the breakpoints were found in 96 patients (70.5%), and those of 10 bp or longer were found in 49 patients (36.0%) (Table 3). It is well known that the common deletion is flanked by 13-bp direct repeats (Schon et al. 1989; Mita et al. 1990). We also found two other common deletions in addition to the most common deletion (34 patients, 25.0%), namely, the 2,310-bp deletion from nt 12113 to nt 14421 (11 patients, 8.0%) and the 7,664-bp deletion from nt 6330 to nt 13993 (ten patients, 7.3%). These additional common deletions had incomplete direct repeats longer than 13 bp with one base mismatch (Fig. 6). Note that the 2,310-bp common deletion was only detected in female patients in this study. Two previous studies describing this deletion provided no information about patient gender (Mita et al. 1990; Deugol et al. 1991).

Discussion

We examined 136 patients with single large-scale deletions in terms of their clinical phenotypes, genomic features, and their relationships. All but three patients were clinically diagnosed as having CPEO, KSS, and PS, which are widely known to be associated with mtDNA deletions. Chronologically, PS is recognized and diagnosed in infants or very young children, and the most prominent clinical feature of

Table 2 Proportion of deletion, age at onset, clinical diagnosis, and clinical manifestations of patients with the common 4,977-bp deletion

Percent del	Onset age (years)	Clinical diagnosis	Clinical manifestation								
			Ptosis	PEO	Retinopathy	Heart conduction block	Deafness	Muscle weakness	Short stature	Anemia	Remarks
20	20	CPEO	○	+	−	−	−	−	−	−	
28	17	CPEO	○	+	−	−	+	+	−	−	
31	36	CPEO	○	+	−	−	+	+	−	−	
37	20	CPEO	○	+	U	−	−	+	+	−	
37	36	CPEO	+	+	−	−	○	+	−	−	
38	31	CPEO	○	+	U	−	−	+	−	−	
40	14	CPEO	○	+	−	−	−	+	+	−	
42	13	CPEO	○	+	U	U	−	−	−	−	
45	25	CPEO	○	+	U	−	−	−	−	−	
50	12	CPEO	○	+	−	−	−	−	−	−	
50	15	CPEO	○	+	U	−	−	+	−	−	
50	26	CPEO	○	+	U	U	U	−	−	−	
51	6	CPEO	○	+	−	−	−	−	−	−	
54	13	CPEO	○	○	U	−	−	−	−	−	
54	28	CPEO	+	○	−	+	−	+	−	−	
56	49	CPEO	○	+	−	+	−	+	−	−	
60	24	CPEO	○	+	U	U	U	+	−	−	
66	14	CPEO	○	+	−	−	−	+	−	−	
70	10	CPEO	○	+	+	−	−	+	−	−	
70	10	CPEO	○	+	−	−	+	−	+	−	
70	12	CPEO	○	+	−	−	−	+	−	−	Dysphagia
75	22	CPEO	○	+	−	−	−	+	−	−	
90	49	CPEO	○	+	+	−	−	+	−	−	
57	8	KSS	○	+	+	+	−	+	+	−	IDDM + ataxia
58	11	KSS	○	+	+	+	+	+	+	−	Ataxia
60	6	KSS	+	+	+	−	+	−	○	−	
64	15	KSS	○	+	+	+	−	+	−	−	
67	13	KSS	○	+	+	+	−	+	−	−	
72	5	KSS	○	+	+	−	+	+	+	−	IDDM
80	11	KSS	○	+	+	−	+	−	+	−	Ataxia
81	11	KSS	○	+	+	+	+	+	−	−	
59	1	Leigh	−	−	−	−	U	○	−	+	Coma
55	1	Pearson	−	−	U	U	U	U	−	+	Thrombocytopenia + diarrhea
82	0 days	Pearson	−	−	U	U	U	U	−	○	

Percent del percent of deleted mitochondrial DNA (mtDNA), *CPEO* chronic progressive external ophthalmoplegia, *KSS* Keans-Sayre syndrome, *Leigh* Leigh syndrome, *Pearson* Pearson's marrow pancreatic syndrome, ○ initial symptom, + presence of manifestation, − absence of manifestation, *U* unknown, *IDDM* insulin-dependent diabetes mellitus

this syndrome is anemia. However, this anemic condition usually disappears by 1 year. There are several reports that PS patients later develop the KSS phenotype (Larsson et al. 1990; McShane et al. 1991; Akman et al. 2004). As for KSS, six out of the eight patients whose age at onset was younger than 5 years and 9 out of all 33 patients were recognized to have short stature as an initial finding. In these patients, ptosis/PEO appeared after a few years from the time when they were given medical attention by pediatricians. Thus, the possibility of mtDNA deletion disorder in such cases without a previous history of anemia must be considered.

We hypothesized that size and location of mtDNA deletion are associated with clinical features. In our previous study, evidence supporting this hypothesis was exiguous because of the small number of patients (Goto

Table 3 Patterns of deletions and direct repeats at breakpoints

Length of direct repeats (bp)	Patterns of deletion	Number of patients
0–3	39	40
4	5	5
5	7	16
6	8	10
7	6	6
8	7	7
9	3	3
10	2	12
11	2	2
12	0	0
13	2	35
Total	81	136

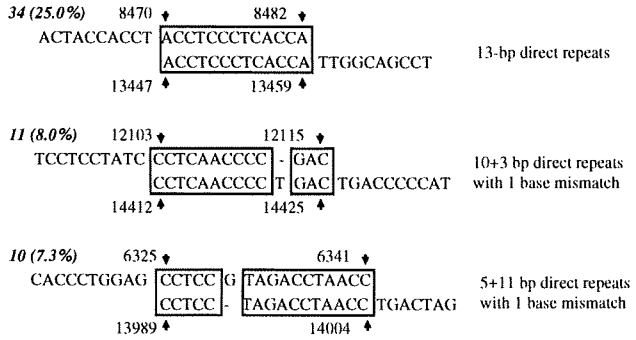

Fig. 6 Sequences at the breakpoints of three major common deletions. Direct repeats are surrounded by *square*, with a nucleotide number based on the standard sequence

et al. 1990a). Aure et al. (2007) divided 69 patients with mtDNA deletion to two groups according to the presence or absence of brain manifestations such as cerebellar ataxia, movement disorder, pyramidal syndrome, or dementia. They found no difference in the size and location of deletion in these two groups. In the study reported here, patients with longer deletions, in which more tRNAs were included, had earlier disease onset. Furthermore, KSS patients had longer deletion and larger number of tRNAs than CPEO patients. Taking age into account, it seems probable to assume that in patients with longer deletion, more deleted tRNAs induce the development of the KSS phenotype or enhance multisystemic involvement. We also found the patients with the deletion, including COX or ATPase subunits, showed earlier onset than those patients with the deletion limited to the region of ND and/or CYB subunits. It may support the relationship between the quality of the deletion and disease severity.

The quality of deletion is not a sole determinant of disease severity. Because patients who had deletion at the common deletion site showed various clinical symptoms (Table 2), we thought that systemic distribution and heteroplasmy (or quantity) of deletion may also be major factors causing clinical variety. The difference between KSS and CPEO is believed to be the extent of tissue or organ involvement. Although KSS is a systemic disorder and CPEO is a muscle-specific disease, these definitions are not strict. Based on Rowland's criteria of KSS, patients have muscular symptoms (ptosis, PEO, muscle weakness), retinopathy, cardiac conduction defects, and central nervous system symptoms or signs (cerebellar signs, high CSF protein concentration due to white-matter degeneration). Because our study showed that short stature and deafness were highly prevalent and IDDM and deToni–Fanconi–Debré syndrome were sometimes prominent manifestations of KSS, these manifestations should be added to the minor items for KSS diagnosis. All CPEO patients except one had ptosis/PEO as initial symptom. Because a substantial proportion of these patients, especially those younger than 20 years, had nonmuscular symptoms, careful assessment of systemic involvement is required in evaluating CPEO patients.

Deletions are usually heteroplasmic, and the proportion varies in each case (Moraes et al. 1989; Goto et al. 1990b) and each tissue (Marzuki et al. 1997). The previous reports and this study showed that there is no correlation between the proportion of deleted mtDNA in skeletal muscle and the age at onset. Aure et al. (2007) reported that the presence and proportion of mtDNA deletion in blood but not in skeletal muscle showed a relationship with severe prognosis in terms of rate of progression, tissular extension, and rate of survival. Because a muscle specimen was not available, we could only examine several blood samples, which were not sufficient for statistic analysis. On the other hand, the distribution of deleted mtDNA at cellular, tissue, and organ levels could not be detect by the method used. The cells with high deletion content might be lost more easily than those with low content (Hayashi et al. 1991). Regarding the relationship between the proportion of deleted mtDNA and clinical severity, the status at examination could be "the area swept by the flames" after loss of cells with high deletion content. It suggests that the remaining cells had a relatively low proportion of deletion despite the severe cell loss, which may directly induce organ symptoms such as muscle weakness. Overall, it is important to understand the mechanism of how deleted mtDNA molecules spread to the whole body or how they are limited to specific cells or tissues. Many factors may be involved in this phenomenon, such as control of replication machinery, presence of duplication, and so on.

Although slip replication (Shoffner et al. 1989) and homologous recombination have been suggested (Deugol et al. 1991), the genomic mechanism of this deletion event

is still unknown. Direct repeats flanking breakpoints have been frequently reported. In our study, 70% of patients had 4-bp or longer direct repeats as those of previous reports (Mita et al. 1990). We emphasize that we detected two additional common deletions besides the most common deletion with 13-bp direct repeats at breakpoints (Schon et al. 1989). These new common deletions also had 13 (10 + 3) and 16 (5 + 11) bp incomplete direct repeats with a mismatch, suggesting that long direct repeats are closely associated with the deletion mechanism.

Only several deletions were found between the origin of heavy-chain replication and that of light-chain replication (from nt 191 to nt 5730), which was called a shorter arc (Moraes et al. 1991; Katayama et al. 1991; Johns and Cornblath 1991; Hammans et al. 1992; Horton et al. 1996; Vu et al. 2000). In our study, there was only one patient with deletion in the shorter arc. Because the same deletion was reported in two studies with three cases, this site might be a hot spot for deletion at the shorter arc. The presence of 13-bp complete direct repeats at these deletion breakpoints further suggests the importance of the length of direct repeats.

In conclusion, our data indicate that initial symptoms other than ptosis/PEO, deletion length, number of deleted tRNAs, and age at onset could be risk factors for systemic involvement of single mtDNA deletion diseases. Deletion of mtDNA has been detected in various neurodegenerative diseases such as Parkinson's disease and Alzheimer's disease (Bender et al. 2006; Kraysberg et al. 2006; Shapira 2006). Further understanding of the mechanism of deletion and its biological importance can lead to the development of a new treatment modality for a particular disease.

Acknowledgments This work was supported by grants-in-aid for scientific research on priority areas from the Ministry of Education, Science, Sports, and Culture of Japan (to YG) and by a grant of the Comprehensive Research Project on Health Sciences Focusing on Drug Innovation (KHD2207) from the Japan Health Sciences Foundation (to YG and IN). We are grateful to Ms. Kumiko Minami, Ms. Mayuko Kato, and Ms. Rika Oketa for technical assistance.

References

Akman CI, Sue CM, Shanske S, Tanji K, Bonilla E, Ojaimi J, Krishna S, Schubert R, DiMauro S (2004) Mitochondrial DNA deletion in a child with megaloblastic anemia and recurrent encephalopathy. J Child Neurol 19:258–261

Aure K, Ogier de Baulny H, Laforet P, Jardel C, Eymard B, Lombes A (2007) Chronic progressive ophthalmoplegia with large-scale mtDNA rearrangement: can we predict progression? Brain 130:1516–1524

Bender A, Krishnan KJ, Morris CM, Taylor GA, Reeve AK, Perry RH, Hersheson JS, Betts J, Klopstock T, Taylor RW, Turnbull DM (2006) High levels of mitochondrial DNA deletions in substantia nigra neurons in aging and Parkinson disease. Nat Genet 38:515–517

Campos Y, Martin MA, Caballero C, Rubio JC, de la Cruz F, Tunon T, Arenas J (2000) Single large-scale mitochondrial DNA deletion in a patient with encephalopathy, cardiomyopathy, and prominent intestinal pseudo-obstruction. Neruomuscul Disord 10:56–58

Deugol F, Nelson I, Amselem S, Romero N, Obermaier-Kusser B, Ponsot G, Marsac C, Lestienne P (1991) Different mechanisms inferred from sequences of human mitochondrial DNA deletions in ocular myopathies. Nucleic Acids Res 19:493–496

Goto Y, Koga Y, Horai S, Nonaka I (1990a) Chronic progressive external ophthalmoplegia: a correlative study of mitochondrial DNA deletions and their phenotypic expression in muscle biopsies. J Neurol Sci 100:63–69

Goto Y, Itami N, KajiiN, Tochimaru H, Endo M, Horai S (1990b) Renal tubular involvement mimicking Bartter syndrome in a patient with Kearns–Sayre syndrome. J Pediatr 116:904–910

Goto Y, Nishino I, Horai S, Nonaka I (1996) Detection of DNA fragments encompassing the deletion junction of mitochondrial genome. Biochem Biophys Res Commun 222:215–219

Hammans SR, Sweeny MG, Wicks DA, Morgan-Hughes JA, Harding AE (1992) A molecular genetic study of focal histochemical defects in mitochondrial encephalomyopathies. Brain 115:343–365

Hayashi J-I, Ohta S, Kikuchi A, Takemitu M, Goto Y, Nonaka I (1991) Introduction of disease-related mitochondrial DNA deletions into HeLa cells lacking mitochondrial DNA results in mitochondrial dysfunction. Proc Natl Acad Sci USA 88:10614–10618

Holt IJ, Harding AE, Morgan-Hughes JA (1988) Deletions of muscle mitochondrial DNA in patients with mitochondrial myopathies. Nature 331:717–719

Horton TM, Petros JA, Heddi A, Shoffner J, Kaufman AE, Graham SD Jr., Gramlich T, Wallace DC (1996) Novel mitochondrial DNA deletion found in a renal cell carcinoma. Genes Chromosomes Cancer 15:95–101

Johns DR, Cornblath DR (1991) Molecular insight into the asymmetric distribution of pathogenetic human mitochondrial DNA deletions. Biochem Biophys Res Commun 174:244–250

Katayama M, Tanaka M, Yamamoto H, Ohbayashi T, Nimura Y, Ozawa T (1991) Deleted mitochondrial DNA in the skeletal muscle of aged individuals. Biochem Int 25:47–56

Kaukonen J, Juselius JK, Tiranti V, Kyttala A, Zeviani M, Comi GP, Keranen S, Peltonen L, Suomalainen A (2000) Role of adenine nucleotide translocator 1 in mtDNA maintenance. Science 289:782–785

Kraysberg Y, Kudryavtseva E, McKee AC, Geula C, Kowall NW, Khrapko K (2006) Mitochondrial DNA deletions are abundant and cause functional impairment in aged human substantia nigra neurons. Nat Genet 38:507–508

Larsson NG, Holme E, Kristiansson B, Oldfors A, Tulinius M (1990) Progressive increase of the mutated mitochondrial DNA fraction in Kearns–Sayre syndrome. Pediatr Res 28:131–136

Marzuki S, Berkovic SF, Saifuddin Noer A, Kapsa RM, Kalnins RM, Byrne E, Sasmono T, Sudoyo H (1997) Developmental genetics of deleted mtDNA in mitochondrial oculomyopathy. J Neurol Sci 145:155–162

McShane MA, Hammans SR, Sweeney M, Holt IJ, Beattie TJ, Brett EM, Harding AE (1991) Pearson syndrome and mitochondrial encephalopathy in a patient with a deletion of mtDNA. Am J Hum Genet 48:39–42

Miller SA, Dykes DD, Polesky HF (1988) A simple salting out procedure for extracting DNA from human nucleated cells. Nucleic Acids Res 16:1215

Mita S, Rizzuto R, Moraes CT, Shanske S, Arnaudo E, Fabrizi GM, Koga Y, DiMauro S, Schon EA (1990) Recombination via flanking direct repeats is a major cause of large-scale deletions of human mitochondrial DNA. Nucl Acids Res 18:561–567

Moraes CT, DiMauro S, Zeviani M, Lombes A, Shanske S, Miranda AF, Nakase H, Bonilla E, Werneck LC, Servidei S, Nonaka I, Koga Y, Spiro AJ, Brownell KW, Schmidt B, Schotland DL, Zupanc M, Devivio DC, Schon EA, Rowland LP (1989) Mitochondrial DNA deletions in progressive external ophthalmoplegia and Kearns–Sayre syndrome. New Engl J Med 320:1293–1299

Moraes CT, Andreetta F, Bonilla E, Shanske S, DiMauro S, Schon EA (1991) Replication-competent human mitochondrial DNA lacking the heavy-strand promoter region. Mol Cell Biol 11:1631–1637

Mori K, Narahara K, Ninomiya S, Goto Y, Nonaka I (1991) Renal and skin involvement in a patient with complete Kearns–Sayre syndrome. Am J Med Genet 38:583–587

Nakai A, Goto Y, Fujisawa K, Shigematsu Y, Kikawa Y, Konishi Y, Nonaka I, Sudo M (1994) Diffuse leukodystrophy with a large-scale mitochondrial DNA deletion. Lancet 343:1397–1938

Nishino I, Spinazzola A, Hirano M (1999) Thymidine phosphorylase gene mutations in MNGIE, a human mitochondrial disorder. Science 283:689–692

Ozawa T, Yoneda M, Tanaka M, Ohno K, Sato W, Suzuki H, Nishikimi M, Yamamoto M, Nonaka I, Horai S (1988) Maternal inheritance of deleted mitochondrial DNA in a family with mitochondrial myopathy. Biochem Biophys Res Commun 154:1240–1247

Poulton J, Deadman ME, Gardiner RM (1989) Duplications of mitochondrial DNA in mitochondrial myopathy. Lancet 1:236–240

Rowland LP (1983) Molecular genetics, pseudogenetics, and clinical neurology. Neurology 33:1179

Rötig A, Colonna M, Bonnefont JP, Blanche S, Fischer A, Saudubray JM, Munnich A (1989) Mitochondrial DNA deletion in Pearson's marrow/pancreas syndrome. Lancet 1:902–903

Schon EA, Rizzuto R, Moraes CT, Nakase H, Zeviani M, DiMauro S (1989) A direct repeat is a hot spot for large-scale deletions of human mitochondrial DNA mutations. Science 244:346–349

Servidei S, Zeviani M, Manfredi G, Ricci E, Silvestri G, Bertini E, Gellera C, Di Mauro S, Di Donato S, Tonali P (1991) Dominantly inherited mitochondrial myopathy with multiple deletions of mitochondrial DNA: clinical, morphologic, and biochemical studies. Neurology 41:1053–1059

Shapira AHV (2006) Mitochondrial disease. Lancet 368:70–82

Shoffner JM, Lott MT, Voljavec AS, Soueidan SA, Costigan DA, Wallace DC (1989) Spontaneous Kearns–Sayre/chronic external ophthalmoplegia plus syndrome associated with a mitochondrial DNA deletion: a slip-replication model and metabolic therapy. Proc Natl Acad Sci USA 86:7952–7956

Spelbrink JN, Li FY, Tiranti V, Nikali K, Yuan QP, Tariq M, Wanrooij S, Garrido N, Comi G, Morandi L, Santoro L, Toscano A, Fabrizi GM, Somer H, Croxen R, Beeson D, Poulton J, Suomalainen A, Jacobs HT, Zeviani M, Larsson C (2001) Human mitochondrial DNA deletions associated with mutations in the gene encoding *Twinkle*, a phage T7 gene 4-like protein localized in mitochondria. Nat Genet 28:223–231

Van Goethem G, Dermaut B, Lofgren A, Martin JJ, Van Broeckhoven C (2001) Mutation of POLG is associated with progressive external opthalmoplegia characterized by mtDNA deletions. Nat Genet 28:211–212

Vu TH, Tanji K, Pallotti F, Golzi V, Hirano M, DiMauro S, Bonilla E (2000) Analysis of mtDNA deletions in muscle by in situ hybridization. Muscle Nerve 23:80–85

Zeviani M, Moraes CT, DiMauro S, Nakase H, Bonilla E, Schon EA, Rowland LP (1988) Deletions of mitochondrial DNA in Kearns–Sayre syndrome. Neurology 38:1339–1346

Zeviani M, Servidei S, Gellera C, Bertini E, DiMauro S, DiDonato S (1989) An autosomal dominant disorder with multiple deletions of mitochondrial DNA starting at the D-loop region. Nature 339:309–311

Journal of Child Neurology
Volume 23 Number 8
August 2008 938-943

10.1177/0883073808315413
http://jcn.sagepub.com
hosted at
http://online.sagepub.com

Progressive Leukoencephalopathy Associated With Aluminum Deposits in Myelin Sheath

M. Itoh, MD, PhD, Y. Suzuki, MD, PhD, K. Sugai, MD, PhD, N. Ozuka, PhD, M. Ohsawa, MD, T. Otsuki, MD, PhD, and Y. Goto, MD, PhD

A 20-year-old woman with progressive leukoencephalopathy developed mental and motor disabilities and fell into a coma after suffering head trauma and febrile episodes from infancy. Brain imaging showed massive abnormal signals in the white matter. The electron spectroscopic imaging of biopsied brain tissue confirmed the electron-dense deposits to be associated with aluminum accumulation in the myelin sheath. Her brain pathology, which showed ferritin- and naphtochrome green-positive deposits, supported the imaging analysis. The clinicopathological features indicate a new form of progressive leukoencephalopathy.

Keywords: leukoencephalopathy; aluminum; electron spectroscopic imaging

Although white matter degeneration can be commonly seen in metabolic diseases or neurodegenerative disorders, cystic or spongy changes are rare. We identified a woman who had episodic neurological and psychotic deterioration associated with enhancing white matter lesions which had progressed to spongy degeneration. The lesions coalesced, rapidly or after periods of remission, destroying larger areas of white matter. Her clinical feature was likely to be leukoencephalopathy with vanishing white matter, which clinically presents with unexplained coma, spastic paresis, ataxia and epilepsy after infection, minor head trauma, as well as pathologically cystic degeneration of the cerebral white matter.[1] Mutation of the subunits of *EIF2B*, the eukaryotic translational initiation factor, is a cause of leukoencephalopathy with vanishing white matter.[2] However, non-*EIF2B*-mutated leukoencephalopathies, which have the same clinical course as VWM, are also reported.[3] Another white matter destructive disease is known as myelinoclastic diffuse sclerosis or Schilder disease.[4] The pathology of myelinoclastic diffuse sclerosis is characterized by destruction of myelin and axon with inflammation. Aluminum-related encephalopathy has also been reported.[5-9] In 4 of 5 reported cases, the cause was found to be aluminum accumulation, but the cause in the other case was unknown. In this study, we report a case of rare aluminum-related leukoencephalopathy without intoxication.

From the National Institute of Neuroscience, National Center of Neurology and Psychiatry (NCNP), Tokyo, Japan (MI, MO, NO, YG); Department of Pediatrics, Aichi Aoitori Medical and Welfare Center, Nagoya, Japan (YS); National Hospital for Mental, Nervous and Muscular Disorders, Tokyo, Japan (KS, TO).

Address correspondence to: M. Itoh, MD, PhD, Department of Mental Retardation and Birth Defect Research, National Institute of Neuroscience, National Center of Neurology and Psychiatry, 4-1-1 Ogawahigashi, Kodaira, Tokyo 187-8502, Japan; phone: 81-423461713; e-mail: itoh@ncnp.go.jp.

Itoh M, Suzuki Y, Sugai K, Ozuka N, Ohsawa M, Otsuki T, Goto Y. Progressive leukoencephalopathy associated with aluminum deposits in myelin sheath. *J Child Neurol.* 2008;23:938-943.

Case Report

A 20-year-old woman was the second child of unrelated parents; the other family members, including her brother and sister, were healthy. After suffering a minor head injury at 6 years of age, she suddenly developed a learning difficulty and showed ataxic gait. At 14 years of age, she suffered from depression and mild mental deterioration. Her deep tendon reflexes showed normal response. Ocular fundi were also normal. Her electroencephalogram (EEG) showed diffuse slow activity without spike waves. The motor conduction velocity of the median nerve was 52.6 m/s (normal range, 54–72 m/s). The first magnetic resonance imaging (MRI) showed diffusely abnormal signals in the cerebral and cerebellar white matter (Figure 1A, B). Her biochemical data were normal, excluding an increase of myelin basic protein in the cerebrospinal fluid (10.1 ng/ml, normal value under 0.1 ng/ml). Extensive metabolic data were normal, including lysosomal and peroxisomal enzyme activities, organic acids, very long chain fatty acids, histoenzymological examination of a muscle biopsy with analysis of respiratory chain enzyme complexes, as well as no lactic acidemia and normal N-acetylaspartate in urine. She had normal levels of thyroid gland and gonad hormones. Her electrophysiological data showed generalized slow activity of EEG and prolonged latency of visual evoked potentials and sensory evoked

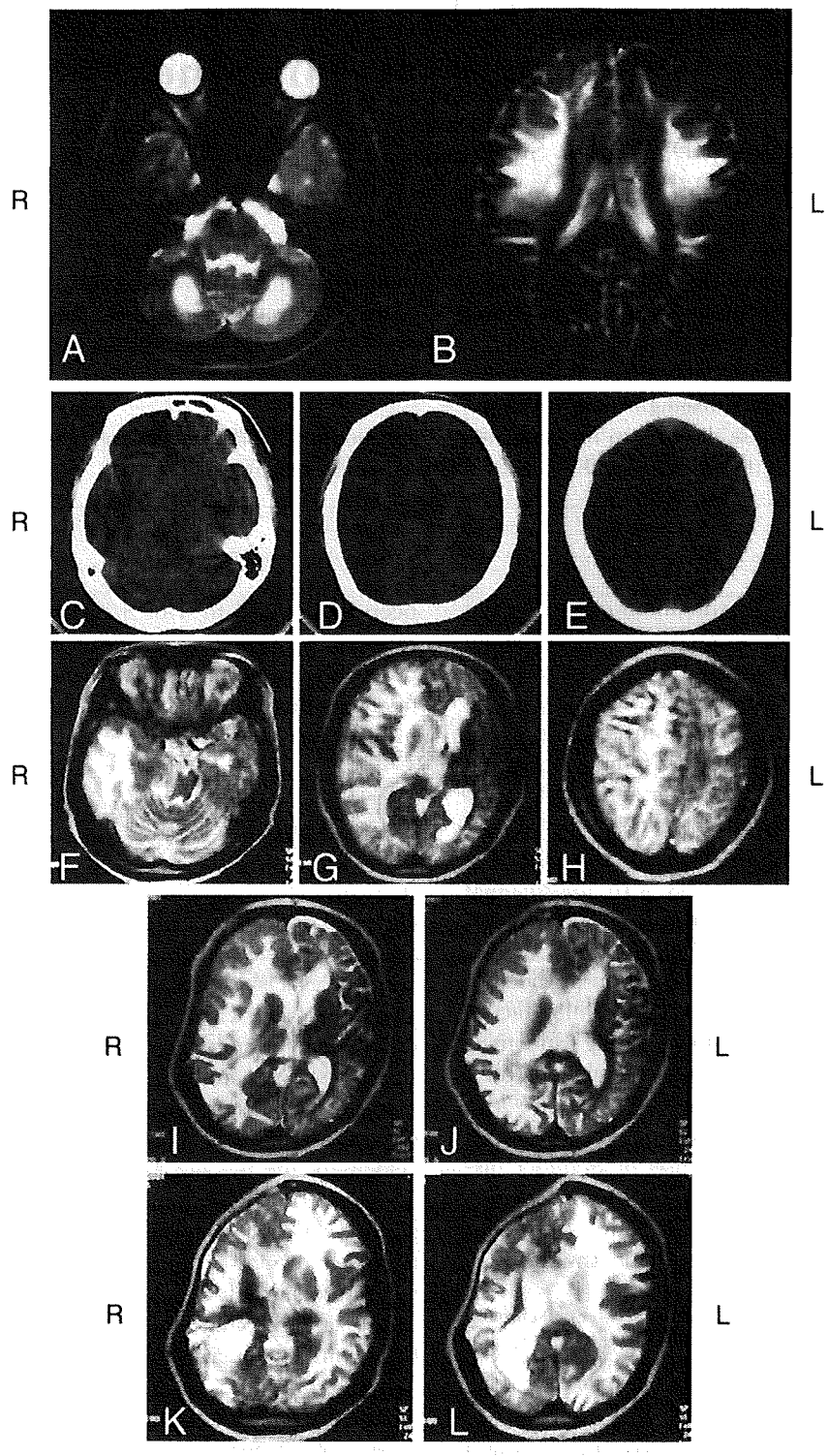

Figure 1. Series of brain magnetic resonance imaging (MRI) and computed tomography scan (CT). The first MRI at 14 years of age shows diffuse white matter abnormalities. The cerebral and cerebellar white matter signal is high-intensity on T2-weighted images (A, B). The CT at 20 years of age shows diffuse low density in the right white matter and midline shift with brain swelling (C–E). At the same time, the second MRI reveals high-intensity on T2-weighted images in the right white matter and massive edema with compression of the brainstem (F–H). Ventricular dilation and cerebellar atrophy are also evident. After surgery, the third MRI demonstrates high-intensity on T2-weighted images in the right white matter and dilation of the bilateral ventricles, but no edema (I, J). Two months after the surgery, the fourth MRI shows expanded high-intensity on T2-weighted images in the left white matter (K, L). R, right; L, left.

potentials. We confirmed no mutation of mitochondrial DNA and all subtypes of *EIF2B*.

At 20 years of age, the patient fell into a coma with anisocoria and left spastic hemiparesis after respiratory infection. Brain computed tomography scan demonstrated extensive hypodensity of the cerebral white matter and MRI revealed diffusely severe edema of the right white matter with midline shift and compression of the brainstem, as well as dilatation of the left lateral ventricle (Figure 1C–H). After she underwent surgery to reduce the pressure on the brain, her consciousness level improved. At that time, a third MRI revealed diffuse abnormal intensity of the right white matter and ventricular dilatation (Figure 1I, J). Two months after the surgery, she developed complete spastic quadriparesis with hyperreflexia and coma after a febrile episode, but did not have cerebellar ataxia or nystagmus. The fourth MRI demonstrated marked loss of white matter and ventricular dilatation in the right hemisphere, and the left hemisphere showed diffusely high intensity of the white matter and slit ventricle with swelling (Figure 1K, L). Her condition was slowly progressive and developed into a vegetative state.

Neuropathology

Brain tissue was removed from the right temporal lobe. The white matter showed a severe spongy and edematous state and diffuse demyelination and rarefaction without inflammatory cell infiltration and pathological reaction (Figure 2A). The oligodendrocytes were slightly decreased in density. However, we did not observe foamy degeneration of oligodendrocyte as seen in leukoencephalopathy with vanishing white matter. Bodian silver impregnation showed normal axons, (Figure 2B). Neurofilament immunoreactivity was also normal (data not shown). We did not observe abnormal PAS-positive deposits or accumulation as in amyloid neuropathy (Figure 2C). According to a previous description,[10] the immunohistochemistry for proteolipid protein (PLP; monoclonal PLP antibody, dilution of 1:100, AGMED, Bedford, MA), myelin basic protein (MBP; polyclonal MBP antibody, dilution of 1:100, DAKO Co., Carpinteria, CA), and myelin 2,3-cyclic nucleotide 3'-phosphodiesterase (CNPase; monoclonal CNPase antibody, dilution of 1:500, Sternberger Monoclonals Inc., Baltimore, MD), showed PLP- and MBP-positive cells and fibers only in the perivascular regions (Figure 2D, E), whereas CNPase-positive cells were diffusely distributed in the white matter (Figure 2F). Additionally, glial fibrillary acidic protein (GFAP; monoclonal GFAP antibody, dilution of 1:5000, Sigma, St. Louis, MO) and CD68 (monoclonal CD68 antibody, dilution of 1:1000, DAKO, Glostrup, Denmark) were positive in the white matter (Figure 2G, H), whereas MAP2 (monoclonal MAP2 antibody, dilution of 1:100, Sigma, St. Louis, MO) was normal (Figure 2I). Also, immunohistochemistry for ferritin (1:1, Biogenesis Ltd., Poole, UK) and histochemistry of naphtochrome green to detect trace elements demonstrated ferritin-immunopositive granules distributed in oligodendrocytes in the white matter (Figure 2G); naphtochrome green-stained fibers and cells were also observed in the white matter (Figure 2H). These facts suggested that aluminum or calcium accumulated in the white matter. Electron microscope examination revealed disruption of the myelin sheath and accumulation of electron-dense deposits in disrupted myelin (Figure 2I). Electron spectroscopic imaging technique confirmed that these deposits were aluminum (Figure 2J, K).[11]

Discussion

Our patient had some clinicopathological characteristics that were clinically leukoencephalopathy with vanishing white matter-like features and pathologically like those of progressive cavitating leukoencephalopathy or myelinoclastic diffuse sclerosis, except for the electron microscopic results. Ferritin-positive deposits and naphtochrome green-stained materials suggested aluminum accumulation.[12] The immunohistochemical findings also supported our electron microscopic appearance. Electron spectroscopy can pick up a characteristic electron voltage as a specific element.[11] Although the baseline signal of aluminum has the same signal level as N (nitrogen), O (oxygen), and Cu (copper) in the P1 point of Figure 2K, the aluminum level in the P2 point obviously increases more than those of N, O, and Cu. Taken together, we determined that many deposits in the myelin sheath contained aluminum, but could not confirm how the aluminum passed through the blood–brain barrier and accumulated in the white matter. Interestingly, gastrointestinal aluminum absorption is increased in patients with Down syndrome, who develop the neuropathological features of Alzheimer disease by early middle age.[13] Also, the gallium–aluminum binding deficiency serves to increase free aluminum in plasma, and this free aluminum could move readily into the brain, where it has neurotoxic effects.[14] Down syndrome shows an induction of the transferrin-binding in plasma with age.[14,15] An excessive accumulation of lactotransferrin, which is a transporter of aluminum, may lead to a cytotoxic effect resulting in the formation of intracellular lesions.[16] We may speculate that the aluminum concentration is controlled by the gastrointestinal absorption and the gallium and transferrin binding activity in plasma. The 2 abnormal systems may combine in the pathogenesis of aluminum accumulation in the brain. Of course, we do not yet fully understand the mechanism of the aluminum accumulation.

Although this unexpected aluminum intake is reportedly associated with normal aging, neurotoxic encephalopathy, and a risk factor of Alzheimer disease,[5-9,17] very few cases of aluminum-related encephalopathy or leukoencephalopathy

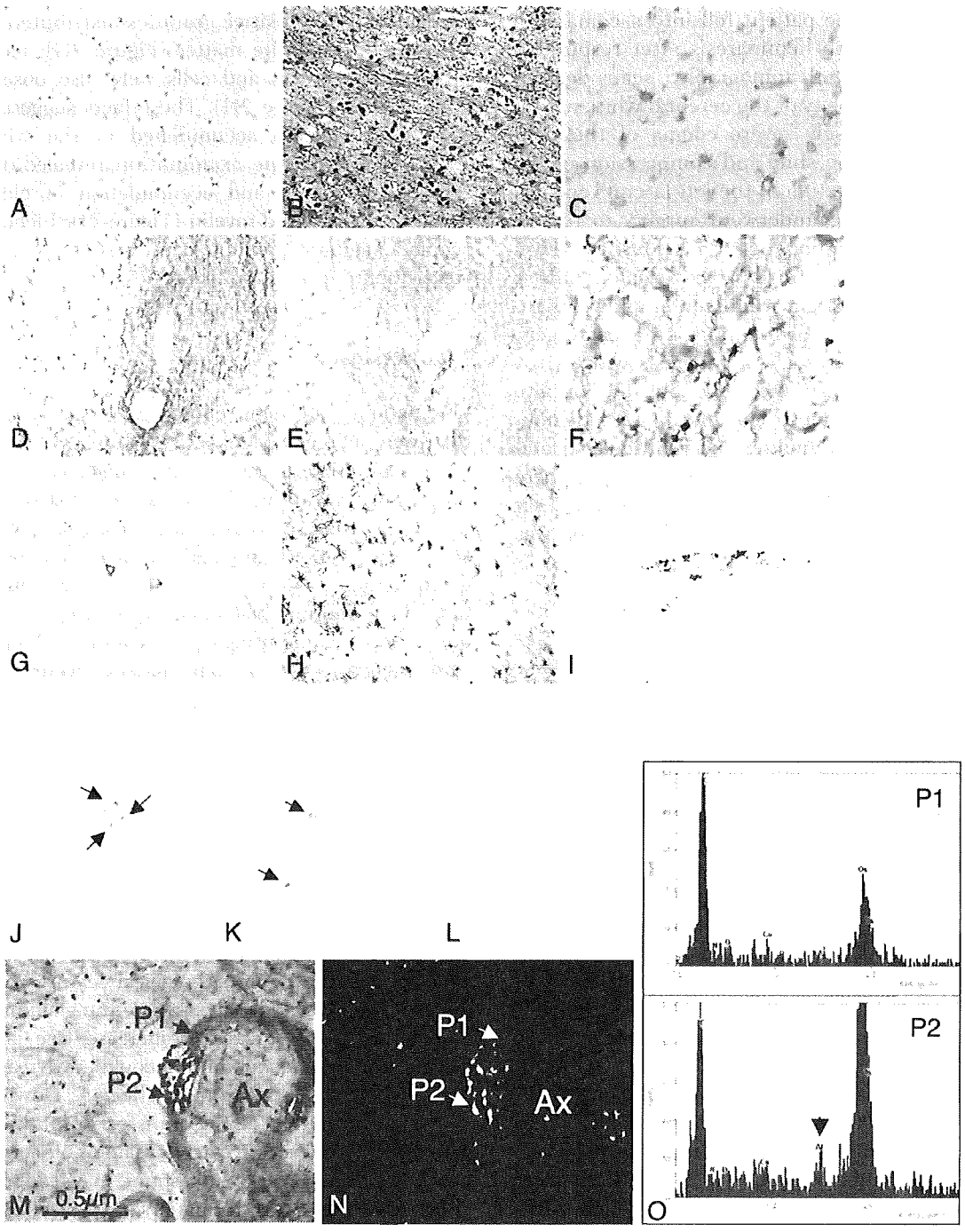

Figure 2. Neuropathological features of the surgical biopsy materials. The right hemispheric white matter appears diffusely affected, with a preservation of myelin (A). The white matter is cystic changes and rarefaction, disruption of myelin; however, axons are relatively normal (A, B). PAS storage is not observed (C). PLP-positive fibers (D) and MBP-positive fibers (E) are observed in the perivascular region. CNPase-positive cells and fibers are scattered, but oligodendrocytes are not decreased (F). As a reactive response, GFAP-positive cells diffusely distributed in the white matter (G) and CD68-positive macrophages are seen in the perivascular space (H), whereas neurons are relatively normal in appearance for MAP2 (I). Ferritin-positive granules in the white matter are observed (arrows in J) and dark green granules locate in cytoplasm (arrow in K). Negative staining with naphtochrome green in normal control white matter (L). Electron microscope shows myelin sheath disruption with electron-dense deposits (M). Aluminum mapping with electron spectroscopic imaging technique reveals these deposits are compatible with aluminum accumulation (N). Electron spectroscope demonstrates no peak in the P1 point in the A (O), but a peak of aluminum spectroscopy level in the P2 (arrow in K). Carbon and osmium are high spectroscopy level in normal. Ax: axon. A, Luxol fast blue and cresyl violet, Klüver-Barrera, staining. B, Bodian silver impregnation. C, PAS staining. D, PLP immunostaining. E, MBP immunostaining. F, CNPase immunostaining. G, GFAP immunostaining. H, CD68 immunostaining. I, MAP2 immunostaining. J, Ferritin immunostaining. K and L, naphtochrome green staining; 11-year-old control white matter (L). M and N, Electron microscope. Original magnifications: A–F ×100, G–I ×200, J–L ×400, M and N ×15 000.

Table 1. Summary of Literature of Aluminum-Related Encephalopathy

Case	Age	Sex	Probable Causes	Symptoms	Al Concentration	Pathology (or MRI Findings)	Reference
1	n.d.	n.d.	Al-containing vaccine	Motor symptoms, cerebellar signs, visual loss, sensory disturbance, cognitive and behavioral problems	n.d.	MS-like features (MRI)	5
2	58 y	f	Al-containing water	Mental deterioration, visual hallucination 15 years later	23.3 μg/g (<2) in cortex	Congophilic angiopathy	6
3	52 y	f	Al-containing cement bone when reconstruction	Loss of consciousness, myoclonic jerks, seizure for 6 months	9.3 μg/g (<2) in cortex	Al-containing argyrophilic inclusions in neurons, glia, and choroid plexus	8
4	59 y	f	3.0 g hydroxyl-Al gel for 15 years	Tremor, delirium for 9 months	195 μg/L (<10) in serum, 12 μg/L (<5) in CSF	Nonspecific mild atrophy, calcification	9
5	37 y	m	Unknown	Mental deterioration for 10 years	n.d.	Patchy demyelination, calcification with Al deposits	7
Our patient	20 y	f	Unknown	Mental deterioration, epilepsy	n.m.	Cystic and spongy white matter, Al deposits in the myelin sheath	

Abbreviations: n.d., not described; Al, aluminum; MS, multiple sclerosis; CSF, cerebrospinal fluid; n.m., not measured.

have been reported (Table 1). One of these reported cases featured leukodystrophy without an aluminum administration history,[7] but the other cases might involve aluminum intoxication.[5,6,8,9] We could not measure her cerebrospinal fluid aluminum concentration. Moreover, the deposits tightly bound to the myelin sheath might not leak into the cerebrospinal fluid.

Myelin is known to easily become a primary target of aluminum toxicity, as aluminum binds to transferrin and is taken into oligodendrocytes.[18,19] This effect could contribute to aluminum-induced toxicity. Oxidative damage following chronic aluminum exposure in adult and pup rat brains has been reported.[20] Aluminum exposure leads to a significant decrease in superoxide dismutase and catalase activity in the brain.[20] Several stresses, including increased body temperature, are also known to induce oxidant cascade activity. Aluminum-induced oxidative damage may have formed spongy white matter degeneration in this case. However, although it is unknown how aluminum accumulated in the myelin sheath, our patient's clinicopathological features may be a new form of progressive leukoencephalopathy.

Acknowledgments

We thank Dr. S. Meshizuka, Tottori University, for his valuable advice regarding aluminum detection in brain tissue, and also Mr. S. Kumagai and Mrs. A. Sakamoto, NCNP, for technical assistance. This study was supported by the Ministry of Health, Welfare and Labor of Japan.

References

1. van der Knaap MS, Kamphorst W, Barth PG, et al. Phenotypic variation in leukoencephalopathy with vanishing white matter. *Neurology.* 1998;51:540-547.
2. Leegwater PA, Vermeulen G, Könst AA, et al. Subunits of the translation initiation factor eIF2B are mutant in leukoencephalopathy with vanishing white matter. *Nat Genet.* 2001; 29:383-388.
3. Naidu S, Bibat G, Lin D, et al. Progressive cavitating leukoencephalopathy: a novel childhood disease. *Ann Neurol.* 2005;58: 929-938.
4. Poser CM, Goutières F, Carpentier MA, Aicardi J. Schilder's myelinoclastic diffuse sclerosis. *Pediatrics.* 1986;77:107-112.
5. Authier FJ, Cherin P, Creange A, et al. Central nervous system disease in patients with macrophagic myofasciitis. *Brain.* 2001; 124:974-983.
6. Exley C, Esiri MM. Severe cerebral congophilic angiopathy coincident with increased brain aluminium in a resident of Camelford, Cornwall, UK. *J Neurol Neurosurg Psychiatry.* 2006;77:877-879.
7. Lapresle J, Duckett S, Galle P, Cartier L. Clinical, anatomical and biophysical data on a case of encephalopathy with aluminum deposits. *C R Seances Soc Biol Fil.* 1975;169:282-285.
8. Reusche E, Pilz P, Oberascher G, et al. Subacute fatal aluminum encephalopathy after reconstructive otoneurosurgery: a case report. *Hum Pathol.* 2001;32:1136-1140.

9. Shirabe T, Irie K, Uchida M. Autopsy case of aluminum encephalopathy. *Neuropathology.* 2002;22:206-210.
10. Shiraishi K, Itoh M, Sano K, et al. Myelination of a fetus with Pelizaeus-Merzbacher disease: immunopathological study. *Ann Neurol.* 2003;54:259-262.
11. Futaesaku Y, Yano M, Ueno M, et al. Principles of electron spectroscopic imaging (ESI) in hard tissue biology. *J Hard Tissue Biol.*1998;7:1-10.
12. Fleming J, Joshi JG. Ferritin: isolation of aluminum-ferritin complex from brain. *Proc Natl Acad Sci USA.* 1987;84:7866-7870.
13. Moore PB, Edwardson JA, Ferrier IN, et al. Gastrointestinal absorption of aluminum is increased in Down's syndrome. *Biol Psychiatry.* 1997;41:488-492.
14. Farrar G, Altmann P, Welch S, et al. Defective gallium-transferrin binding in Alzheimer disease and Down syndrome: possible mechanism for accumulation of aluminium in brain. *Lancet.* 1990;335:747-750.
15. Hodgkins PS, Prasher V, Farrar G, Armstrong R, Sturman S, Corbett J, Blair JA. Reduced transferring binding in Down syndrome: a route to senile plaque formation and dementia. *Neuroreport.* 1993;5:21-24.
16. Leveugle B, Spik G, Perl DP, et al. The iron-binding protein lactotransferrin is present in pathologic lesions in a variety of neurodegenerative disorders: a comparative immunohistochemical analysis. *Brain Res.* 1994;650:20-31.
17. Miu AC, Olteanu AI, Miclea M. A behavioral and ultrastructural dissection of the interference of aluminum with aging. *J Alzheimers Dis.* 2004;6:315-328.
18. Verstraeten SV, Golub MS, Keen CL, Oteiza PI. Myelin is a preferential target of aluminum-mediated oxidative damage. *Arch Biochem Biophys.* 1997;344:289-294.
19. Golub MS, Han B, Keen CL. Aluminum uptake and effects on transferrin mediated iron uptake in primary cultures of rat neurons, astrocytes and oligodendrocytes. *Neurotoxicology.* 1999;20:961-970.
20. Nehru B, Anand P. Oxidative damage following chronic aluminium exposure in adult and pup rat brains. *J Trace Elem Med Biol.* 2005;19:203-208.

J Neuropathol Exp Neurol

Vol. 66, No. 2
February 2007
pp. 117–123

ORIGINAL ARTICLE

Methyl CpG-Binding Protein 2 (a Mutation of Which Causes Rett Syndrome) Directly Regulates Insulin-Like Growth Factor Binding Protein 3 in Mouse and Human Brains

Masayuki Itoh, MD, PhD, Shuhei Ide, MD, Sachio Takashima, MD, PhD, Shinichi Kudo, MD, PhD, Yoshiko Nomura, MD, PhD, Masaya Segawa, MD, PhD, Takeo Kubota, MD, PhD, Hideo Mori, MD, PhD, Shigeki Tanaka, MD, PhD, Hiroshi Horie, MD, PhD, Yuzo Tanabe, MD, PhD, and Yu-ichi Goto, MD, PhD

Abstract

Rett syndrome (RTT) is a major neurodevelopmental disorder, characterized by mental retardation and autistic behavior. Mutation of the *MeCP2* gene, encoding methyl CpG-binding protein 2, causes the disease. The pathomechanism by which MeCP2 dysfunction leads to the RTT phenotype has not been elucidated. We found that MeCP2 directly regulates expression of *insulin-like growth factor binding protein 3* (*IGFBP3*) gene in human and mouse brains. A chromatin immunoprecipitation assay showed that the *IGFBP3* promoter contained an MeCP2 binding site. *IGFBP3* overexpression was observed in the brains of *mecp2*-null mice and human RTT patients using real-time quantitative polymerase chain reaction and Western blot analyses. Moreover, *mecp2*-null mice showed a widely distributed and increased number of IGFBP3-positive cells in the cerebral cortex, whereas wild-type mice at the same age showed fewer IGFBP3-positive cells. These results suggest that *IGFBP3* is a downstream gene regulated by MeCP2 and that the previously reported *BDNF* and *DLX5* genes and MeCP2 may contribute directly to the transcriptional expression of *IGFBP3* in the brain. Interestingly, the pathologic features of *mecp2*-null mice have some similarities to those of *IGFBP3*-transgenic mice, which show a reduction of early postnatal growth. IGFBP3 overexpression due to lack of MeCP2 may lead to delayed brain maturation.

From the Department of Mental Retardation and Birth Defect Research (MI, SI, YG), National Institute of Neuroscience, National Center of Neurology and Psychiatry, Tokyo, Japan; Yanagawa Institute for Developmental Disabilities (S. Takashima), International University of Health and Welfare, Fukuoka, Japan; Department of Biological Science (SK), Hokkaido Institute of Public Health, Sapporo, Japan; Segawa Neurological Clinic for Children (YN, MS), Tokyo, Japan; Department of Epigenetic Medicine (TK), University of Yamanashi, Yamanashi, Japan; Department of Neurology (HM), Juntendo University School of Medicine, Tokyo, Japan; Department of Neurology (S. Tanaka), Juntendo University Urayasu Hospital, Chiba, Japan; and Chiba Children's Hospital (HH, YT), Chiba, Japan.

Send correspondence and reprint requests to: Masayuki Itoh, MD, PhD, Department of Mental Retardation and Birth Defect Research, National Institute of Neuroscience, National Center of Neurology and Psychiatry, 4-1-1 Ogawahigashi, Kodaira, Tokyo 187-8502, Japan; E-mail: itoh@ncnp.go.jp

This study was supported by research grants for Nervous and Mental Disorders from the Ministry of Health, Labor and Welfare of Japan (15B-3 and 18A-3) and from the Ministry of Education, Culture, Science, Sports and Technology of Japan (18390304).

Key Words: Insulin-like growth factor binding protein 3, Methyl CpG-binding protein 2, Rett syndrome.

INTRODUCTION

Methyl CpG-binding protein-2 (MeCP2) serves as a major transcription repressor by forming a complex with histone deacetylase and Sin3A (1–3). Mutation of *MeCP2* causes an X-linked neurodevelopmental disorder, Rett syndrome (RTT) (4), and is also found in some patients with Angelman syndrome (5, 6). Patients with these diseases have shown severe mental retardation, autistic behavior, and intractable seizures. Interestingly, most of the symptoms appear in early childhood, not at birth. Patients with RTT, *MeCP2*-affected girls, typically show normal features for 6 to 18 months and then develop impaired motor skills, stereotypic hand movements, abnormal breathing, microcephaly, and other symptoms. *Mecp2*-null mice show normal development until 4 to 5 weeks of age, and by 6 weeks they present serious neurologic symptoms and die at approximately 8 weeks after birth. These symptoms of both human RTT patients and *mecp2*-null mouse are thought to be due to a deficiency in the brain, although MeCP2 is ubiquitously expressed. This hypothesis is supported by some studies that show a high expression level of MeCP2 in the brain, specifically in neurons (7–9). To understand the mechanism forming these diseases, we must clarify the role direct MeCP2-downstream genes have. Recently, a few MeCP2-downstream genes have been identified, such as *brain-derived neurotrophic factor* (*BDNF*) and *DLX5*, which locate in neuronal cells and are thought to play an important role in early brain development (10–12). Besides these genes, altered expressions of imprinted *UBE3A* and *GABRB3* genes in mice and RTT patients have been reported (13). However, how these genes contribute to form the RTT phenotype is still unknown.

It has recently been reported that downregulation of *insulin-like growth factor binding 3* (*IGFBP3*) due to methylation in association with MeCP2 leads to proliferation of cancer cells in various types of cancers, such as non-small

cell carcinoma of lung, hepatoma, and colorectal cancer, and that overexpression of IGFBP3 inhibits cancer cells proliferation and migration (14–16). IGFBP3 is known to be an antagonist of insulin-like growth factor (IGF) 1 and IGF-2, because its major function is binding to them and carrying them to the target tissues (17). Moreover, *IGFBP3*-transgenic mice show growth retardation in the brain at the early postnatal period and poor neuronal dendritic expansion (18). We can presuppose that *IGFBP3*-transgenic mice in the early postnatal period have poor dendritic expansion of neurons, a feature similar to RTT. Taking these facts together, we can speculate that IGFBP3 is necessary for cellular and neuronal maturation and that IGFBP3 is regulated by MeCP2, not only in malignant cells but also in normal neuronal cells. In the present study, we investigated the correlation between MeCP2 and IGFBP3 to clarify whether *IGFBP3* may also be an important gene for neuronal development as a new MeCP2-downstream gene. Our findings demonstrate that overexpression of *IGFBP3* directly contributes to the neurologic phenotypes associated with MeCP2 deficiency.

MATERIALS AND METHODS

Mouse and Tissue Preparation

B6.129P2(C)-Mecp2$^{tm1.1Bird/J}$ mice lacking exons 3 and 4 were obtained from The Jackson Laboratory (Bar Harbor, ME) and subsequently bred in our institute. We used 10 or more generated mice in this study. The *mecp2*-null, hemizygous (*mecp2*$^{-/y}$) male mice showed initial symptoms such as hindlimb grasping and hypoactivity at approximately 4 weeks of age and died at 8 or 9 weeks of age (19). *Mecp2*$^{-/y}$ and wild-type male littermates, as controls, were used at postconceptual days 12.5 (E12.5), and 17.5 (E17.5), as well as postnatal days 0 (P0), 28 (P28), and 60 (P60). We also used *mecp2*-heterozygous (*mecp2*$^{+/-}$) mice, aged P28. Five animals were obtained from each group for histochemistry and four for RNA expression analyses. The mice were deeply anesthetized under diethyl ether and transcardially perfused with heparin-saline and 4% paraformaldehyde in 0.1 mmol/L PBS, pH 7.4, for histologic study. For expression study, unfixed brains were removed and stored at −80°C until use. This study was approved by the Ethical Committee for Animal Experiments in our institute.

Chromatin Immunoprecipitation Assay

A chromatin immunoprecipitation assay with an antibody against MeCP2 was performed as described previously (20). Cell suspensions from mice cortices were fixed in 1% formaldehyde at room temperature for 10 minutes. After being sonicated and lysated, an aliquot of each sample was removed and used in polymerase chain reaction (PCR) analysis as follows (20). The remainder of the soluble chromatin was incubated at 4°C overnight with a rabbit anti-MeCP2 polyclonal antibody (provided by Dr. S. Kudo, Hokkaido Institute of Public Health, Hokkaido, Japan) (21) as "+," and without the antibody as "−." The purified DNA was analyzed by PCR. The primer sets of mouse *IGFBP3* promoter were used. A forward sequence was CAGGTGCC CGGTGAAGAC, and a reverse sequence was ATATATA GAAGCCGGGGTGG. These were amplified for 35 cycles of 94°C for 30 seconds, 55°C for 30 seconds, and 72°C for 30 seconds. The sequence of mouse *IGFBP3* promoter was obtained from GenBank (accession number AL607124).

For human *IGFBP3* promoter analysis we used the reported primers and reaction condition (15). The PCR primer set was CGTGAGCACGAGGAGCAGGTG (forward sequence) and CAGGAGTGGGGGTTGGGAG (reverse sequence). PCR conditions were 32 cycles of 94°C for 30 seconds, 62°C for 1 minute, and 72°C for 1 minute.

Reverse Transcriptase–PCR and Real-Time Quantitative PCR

After isolation of 1 μg of total RNA of the cerebral cortices using an RNeasy Mini Kit (QIAGEN, Valencia, CA), we carried out reverse transcription with the First-Strand cDNA Synthesis Kit (Amersham Pharmacia Biotech, Piscataway, NJ) or TaqMan Reverse Transcription Reagents (Applied Biosystems, Foster City, CA). To confirm developmental expression of mouse *IGFBP3* mRNA, we performed reverse transcriptase–PCR using a primer set for *IGFBP3* (forward sequence of TGAGTCCGAGGAGGAG CACAA and reverse sequence of TACGTCGTCTTT CCCCTTGGT) and for *β-actin* (forward sequence of TCTGGAAAGCTGTGGCGTGAT and reverse sequence of TTGG AGGCCATGTAGGCCAT) as a reference. One nanogram of each reverse-transcripted cDNA was used under the amplification condition of 35 cycles of 94°C for 30 seconds, 60°C for 30 seconds, and 72°C for 30 seconds.

For quantitative analysis we carried out PCR amplifications with Universal PCR Master Mix (Applied Biosystems) according to the manufacturer's protocol in a real-time ABI PRISM 7700 Instrument (Applied Biosystems). The samples used were wild-type and *mecp2*$^{-/y}$ male mice aged P28. Primers and probes for mouse *MAP2*, *IGFBP3*, and *BDNF* are available from Applied Biosystems. For each genotype, wild-type, and *mecp2*$^{-/y}$ male, four pools of RNA were analyzed: four forebrain RNA preparations per pool. Each 30 ng of reverse-transcripted cDNA was applied. The data obtained were compared by real-time PCR analysis, using *MAP2* mRNA as an internal control and *β-actin* mRNA as a reference. Results were displayed relative to *β-actin* cDNA amounts and statistically compared using the Student *t*-test.

Immunohistochemistry and Immunoblot Analyses of Mice Brains

We made a series of cryosections of brain tissues at 10-μm thickness, stained with Nissl (Sigma, St. Quentin Fallavier, France) and immunostained with a mouse monoclonal antibody against IGFBP3 (Granzyme-Techne, Minneapolis, MN) according to the manufacturer's instructions. Additionally, we performed immunohistochemistry on a rabbit polyclonal MeCP2 antibody, as previously reported (21), at a dilution of 1:3000. These antibodies were already reported to have the epitope-specific reaction (15, 21).

Protein extraction from prepared tissues was carried out by a previous described procedure (22). After transfer to

TABLE. Clinicopathologic Summary of Patients With Rett Syndrome and Controls

Patients	Age (years)	Sex	MeCP2 Mutation	MeCP2 Expression*		Symptoms	Cause of Death	Origin of Subject
				IHC	IB			
RTT								
RTT-1	10	F	R270X	ND	−	RTT	Unknown	HBTRC
RTT-2	24	F	R255X	ND	−	RTT	Respiratory failure	HBTRC
RTT-3	8	F	R255X	ND	−	RTT	Drowning	HBTRC
RTT-4	32	F	P302H	−	−	RTT	Sudden death	Japan
RTT-5	12	F	NE	−	−	RTT	Pneumonia	Japan
RTT-6	14	F	NE	−	ND	RTT	Accident	Japan
Control								
CTL-1	15	F	NE	+	+	ALL	Pneumonia	Japan
CTL-2	16	F	NE	+	+	AML	Pneumonia	Japan
CTL-3	12	M	NE	+	+	AMI	AMI	Japan
CTL-4	31	F	NE	+	+	CbH	CbH	Japan

*, Results of immunohistochemistry (IHC) and immunoblotting (IB) of the brain tissues. + indicates positive reaction; − indicates negative reaction.
ND, not done; RTT, Rett syndrome; HBTRC, tissue from the Harvard Brain Tissue Resource Center; NE, not examined; ALL, acute lymphoblastic leukemia; AML, acute myeloblastic leukemia; AMI, acute myocardial infarction; CbH, cerebellar hemorrhage.

a nylon membrane, we detected IGFBP3-immunoreacted bands using an enhanced chemiluminescence system (Amersham Pharmacia Biotech), according to the manufacturer's instructions. As a reference, microtubule-associated protein 2 (MAP2) and β-actin were detected by the specific antibodies (Sigma).

Immunohistochemistry and Immunoblot Analyses of Human Brains

The human materials used (6 RTT patients and 4 controls) are summarized in the Table. All RTT patients had a clinically classical course. Four RTT patients had MeCP2 mutations in the transcription repression domain of its exon

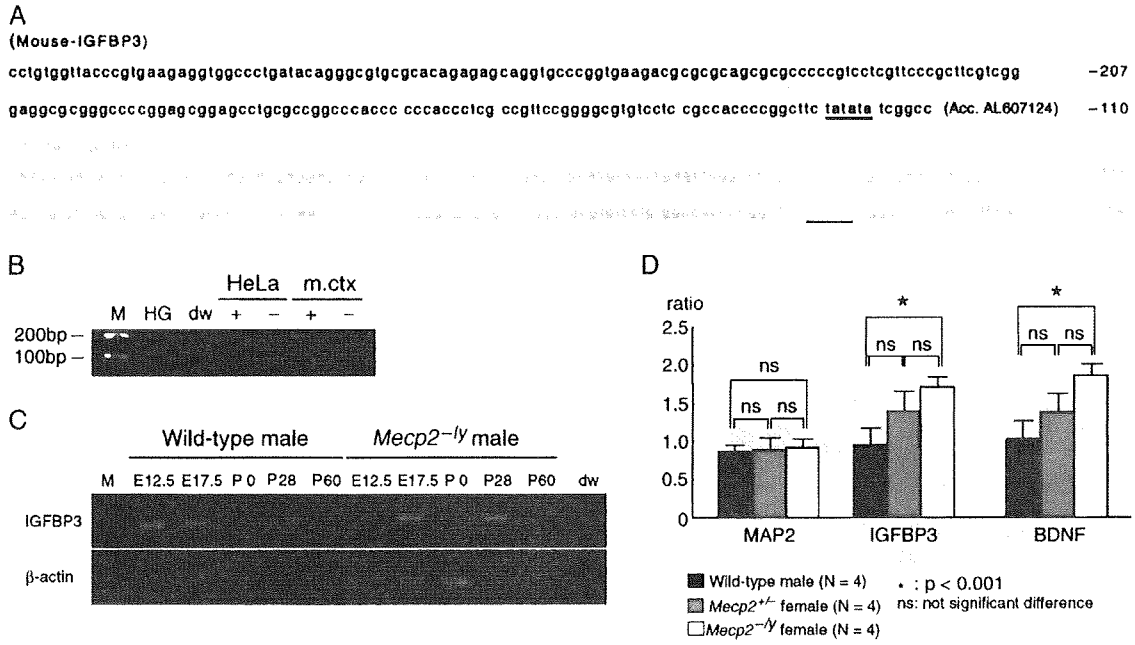

FIGURE 1. Mouse and human *insulin-like growth factor binding protein 3* (*IGFBP3*) promoter sequence and analyses of *IGFBP3* and *MeCP2* in brains. **(A)** Within -500 bp from exon 1, there are CG-rich regions and TATA box (underlines). Black letters indicate a mouse sequence (AL607124) and gray a human sequence (M35878). **(B)** Chromatin immunoprecipitation reaction reveals anti-MeCP2 antibody binding samples (+) and unbinding samples (−) of both HeLa cells, and mouse brain is positive. **(C)** Reverse transcriptase-polymerase chain reaction (PCR) shows *IGFBP3* mRNA of mouse brains developmentally. **(D)** Real-time PCR shows *IGFBP3* of *mecp2*$^{-/y}$ mice significantly increased compared with that of wild-type mice at age postnatal day 28. In *mecp2*$^{+/-}$ brain, *IGFBP3* and *BDNF* expression also increased more than those of wild-type mice; however, there were no significant differences. The y axis indicates each gene expression ratio against *β-actin* as a standard. HG, genomic DNA of HeLa cells; dw, distilled water; M, molecular weight marker; m.ctx, mouse cerebral cortex.